

Testing the starburst/AGN connection with SWIRE X-ray/ $70\mu\text{m}$ sources

M. Trichas^{1*}, A. Georgakakis², M. Rowan-Robinson¹, K. Nandra¹, D. Clements¹,
M. Vaccari³

¹*Astrophysics Group, Blackett Laboratory, Imperial College London, Prince Consort Road, London SW7 2BW, UK.*

²*National Observatory of Athens, I. Metaxa & V. Pavlou, Athens 15236, Greece*

³*Department of Astronomy, University of Padova, Vicolo Osservatorio 5, I-35122 Padua, Italy*

Accepted 23 June 2009

ABSTRACT

We explore the nature of X-ray sources with $70\mu\text{m}$ counterparts selected in the SWIRE fields ELAIS-N1, Lockman Hole and Chandra Deep Field South, for which Chandra X-ray data are available. A total of 28 X-ray/ $70\mu\text{m}$ sources in the redshift interval $0.5 < z < 1.3$ are selected. The X-ray luminosities and the shape of the X-ray spectra show that these sources are AGN. Modelling of the optical to far-infrared Spectral Energy Distribution indicates that most of them (27/28) have a strong starburst component ($> 50 M_{\odot} \text{yr}^{-1}$) that dominates in the infrared. It is found that the X-ray and infrared luminosities of the sample sources are broadly correlated, consistent with a link between AGN activity and star-formation. Contrary to the predictions of some models for the co-evolution of AGN and galaxies, the X-ray/ $70\mu\text{m}$ sources in the sample are not more obscured at X-ray wavelengths compared to the overall X-ray population. It is also found that the X-ray/ $70\mu\text{m}$ sources have lower specific star-formation rates compared to the general $70\mu\text{m}$ population, consistent with AGN feedback moderating the star-formation in the host galaxies.

Key words: galaxies: starburst - galaxies: quasars - X-rays: galaxies - infrared: galaxies

1 INTRODUCTION

A major recent development in extragalactic astronomy is the discovery that a large fraction of the spheroids in the local Universe contain a super-massive black hole (Magorrian et al. 1998). Moreover, the black hole mass is tightly correlated to the stellar mass of the host galaxy bulge (eg Ferrarese et al. 2000; Gebhardt et al. 2000), suggesting that the formation and evolution of galaxies and the build-up of the super-massive black holes at their centers are interconnected. The physical process behind this fundamental observation is under debate, with AGN-driven feedback mechanisms proposed as a plausible option.

Recent simulations which include AGN feedback and postulate that AGN form during galaxy mergers (Hopkins et al. 2005; 2007) have received much attention recently because of their success in reproducing a range of observed properties of both AGN (e.g. duty-cycle, N_{H} distribution; Hopkins et al. 2005) and galaxies (e.g. bimodality of the colour-magnitude relation; Blanton 2006). In this scenario galaxy interactions

trigger the AGN and also produce nuclear starbursts that both feed and obscure the central engine for most of its active lifetime. AGN-driven outflows (i.e. feedback) eventually develop, which at later stages become strong enough to rapidly quench the star-formation, leaving behind a red, passive remnant and allowing the AGN to shine unobscured for a short period ($\approx 10^8$ yr).

A prediction of these simulations is that there should be an association between AGN and starburst events. Examples of such composite objects are rather isolated in the literature however (Cid Fernandes et al. 2001; Page et al. 2004; Alexander et al. 2005), particularly at $z \approx 1$, close to the peak of the AGN luminosity density in the Universe (Barger et al. 2005; Hasinger et al. 2005). This observational fact may point to a more complex AGN/starburst connection than that adopted in current models. For example, observations show that X-ray and/or optically-selected AGN are often found in red early-type bulge-dominated galaxies (Grogan et al. 2002; Pierce et al. 2006; Nandra et al. 2007) with evidence for star-formation events that have terminated in the recent past (Kauffmann et al. 2003 but see Silverman et al. 2009). These observations are consistent with a time lag be-

* Email: m.trichas@imperial.ac.uk

Table 1. X-ray/70 μ m sample

object no.	RA	dec	z^a	L_{cirr}^b	L_{sb}^c	L_{tor}^d	L_{opt}^e	type ^f	A_V^g	lgL_X^h	$\log N(H)^i$
N1											
1	242.03664	54.94373	(0.862)		12.70 (A220)	11.45	11.20	Sbc		43.66	23.56
2	242.14854	54.39154	1.300			12.73	12.82	QSO	0.15	44.41	22.46
3	242.30495	53.90828	0.9923		11.87	12.17	12.32	QSO		45.06	21.61
4	242.45093	54.60308	0.8730		12.01	10.41	11.31	Sbc	0.2	43.84	23.67
5	242.55586	55.11386	(0.542)		11.85 (A220)	11.00	11.10	Sbc		42.87	22.89
6	242.74052	54.68533	(1.270)		12.45	11.85	11.45	Sbc		43.81	21.71
7	242.80289	55.13984	1.280		12.45	11.95	11.75	Sbc		44.68	23.60
8	243.26450	54.72134	(1.138)		12.34	11.20	11.61	Scd		43.58	20.11
Lockman											
1	161.13074	59.09380	1.312		12.91	12.51	12.61	QSO	0.10	44.09	22.79
2	161.19244	58.82482	(1.280)		12.29		11.35	Scd	0.3	43.21	19.83
3	161.01555	58.98413	(1.208)		12.14		11.14	sb	0.6	43.18	22.38
4	160.84180	58.82229	(1.051)		12.01	10.44	11.59	Scd		43.43	19.83
5	160.97850	58.98404	(1.004)		12.00		11.25	Scd	0.1	43.07	23.65
6	161.05058	58.91622	(0.845)		11.94 (A220)		11.64	E		43.43	22.79
7	161.96295	58.86107	(0.762)		12.30		11.60	E		42.81	21.87
8	160.84120	59.21511	(0.754)		11.79	10.50	11.50	Scd		41.98	21.42
9	160.85416	59.28613	(0.690)		11.58	11.08	10.98	Scd		43.35	23.43
10	161.76088	58.75598	(0.644)		11.70 (A220)		10.78	Scd	1.0	43.35	22.38
11	160.72220	59.17268	(0.614)	11.96			11.63	Scd	1.2	42.94	22.37
12	161.21414	59.32958	0.463		11.33	10.93	11.23	sb	0.2	43.60	22.45
13	161.03317	58.74367	0.555		11.76	11.56	11.10	Sbc	0.2	42.25	22.54
14	161.24121	58.56060	(0.905)		12.11 (A220)	10.44	11.46	sb		42.99	22.56
15	161.27065	58.99651	0.264		10.57		9.77	Sab		42.83	23.74
CDFS											
1	52.84087	-27.85638	(1.032)		12.42 (A220)	12.32	11.02	sb		43.20	23.30
2	52.87523	-27.93405	(0.660)		11.98 (A220)		11.53	Scd	0.2	41.74	19.85
3	52.95019	-27.80056	(1.080)		12.33 (A220)	11.13	10.33	sb		42.25	19.84
4	53.01069	-28.05587	(1.158)		12.24	11.64	11.06	Scd		43.60	19.89
5	53.02176	-28.07097	(0.675)		11.58	11.32	10.90	Scd		42.98	22.48

^a Photometric redshifts are denoted in brackets

^b cirrus luminosity

^c starburst luminosity

^d dust torus luminosity

^e Bolometric optical luminosity

^f Optical SED best fit

^g extinction

^h Hard band (2 – 10 keV) X-ray Luminosity in erg s^{-1}

ⁱ Intrinsic column density in cm^{-2}

tween the peak of the star-formation and the BH accretion in these systems.

Alternatively, observational effects may bias our understanding of the properties of AGN hosts. A major problem in assessing the level of star-formation in AGN is the difficulty in decomposing the stellar from the AGN emission, especially in the case of dust enshrouded systems. Combining X-ray data with longer far-IR wavelengths (e.g. 70 μ m) can provide a handle on this issue. The X-rays provide the most efficient way of identifying active BHs, least biased by obscuration, while common wisdom has it that the far-IR is a clean star-formation diagnostic. The sample, which is by no means complete, presented in this paper, has been compiled based on the above criteria: objects close to the peak of the AGN luminosity density which have both X-ray and 70 μ m detections, represents the best candidates for composite objects. Because of instrumental limitations (e.g. sensitivity, confusion), any sample selected at $> 70\mu\text{m}$, like

the one proposed here, represents the brightest and rarest examples of an underlying population that future more sensitive surveys with Herschel will unveil.

2 DATA

The sample of X-ray sources with 70 μ m counterparts studied in this paper is compiled from the SWIRE survey (Lonsdale et al. 2003), one of the largest Spitzer legacy programmes. It covers a total area of 49deg² spread in 6 different fields. The observations have been carried out in all seven photometric bands available to Spitzer, the IRAC 3.6, 4.5, 5.8 and 8 μ m bands (Fazio et al. 2004) and the MIPS 24, 70 and 160 μ m bands (Rieke et al. 2004). The typical 5 σ sensitivities is about 3.7, 5.3, 48, 37.7 μJy in the IRAC 3.6, 4.5, 5.8 and 8 μ m bands respectively. The corresponding 5 σ limits for the MIPS bands are 230 μJy at 24 μ m and

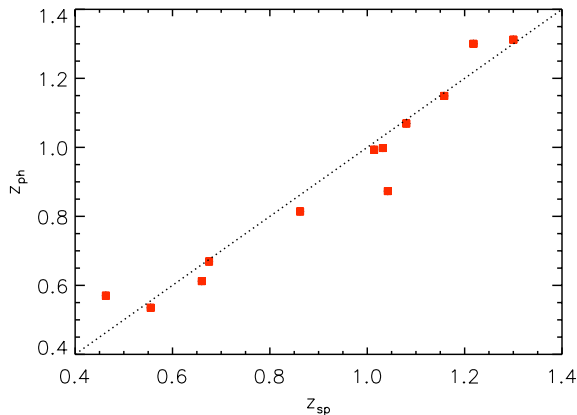


Figure 1. Photometric against spectroscopic redshift estimates for the X-ray/70 μ m sources. Photometric redshifts are estimated using the SED fitting method described in the text. Spectroscopic redshifts are from either our own follow-up program (Trichas et al. in prep) or from the literature. The diagonal line corresponds $z_{phot} = z_{spec}$.

20, 120 mJy at 70 and 160 μ m (Surace et al., 2005). Optical observations in at least 3 photometric bands are available for most of the SWIRE area (>70%). The optical data combined with the SWIRE mid- and far-IR photometry have been used to fit the observed SEDs with a combination of galaxy and AGN templates (Babbedge et al. 2004; Rowan-Robinson et al. 2005) in order to study the nature of infrared selected populations and to estimate photometric redshifts for over 1 million sources (Rowan-Robinson et al. 2008). Details about the latest SWIRE data release can be found in Surace et al. (2005). In this paper we have used multiwavelength data from three SWIRE fields that have X-ray data available from Chandra. These are the ELAIS-N1, the Chandra Deep Field South (CDFs) and the Lockman field. The overlap between the Chandra X-ray observations and the SWIRE survey in these three fields is about 2.5 deg². Details about individual fields are listed below.

2.1 ELAIS-N1

The entire 9 deg² area of SWIRE ELAIS-N1 field has been observed at optical wavebands as part of the Wide Field Survey (WFS, McMahon et al., 2001) using the Wide Field Camera (WFC) on the Isaac Newton Telescope (INT). The survey consists of 600 s exposures in five bands: U, g^r, r^r, i^r and Z to magnitude (Vega, 5 σ for a point-like object) limits of: 23.4, 24.9, 24, 23.2, 21.9 mag respectively. The overall photometric accuracy of the INT WFS survey is 2%. Further details are given in Babbedge et al. (2004) and Surace et al. (2005).

X-ray coverage of ELAIS-N1 consists of two Chandra surveys. The first one is our own, and consists of 30 \times 5 ks exposures with the ACIS-I instrument. There is significant overlap between adjacent ACIS-I pointings, thereby providing nearly even coverage over a circular area of about 1.5 deg². This survey has not been fully presented in a previous publication, except briefly in Georgakakis et al. (2008), and therefore we will describe it in some detail here. The data were obtained in VFaint mode during Cycle 6, between Decem-

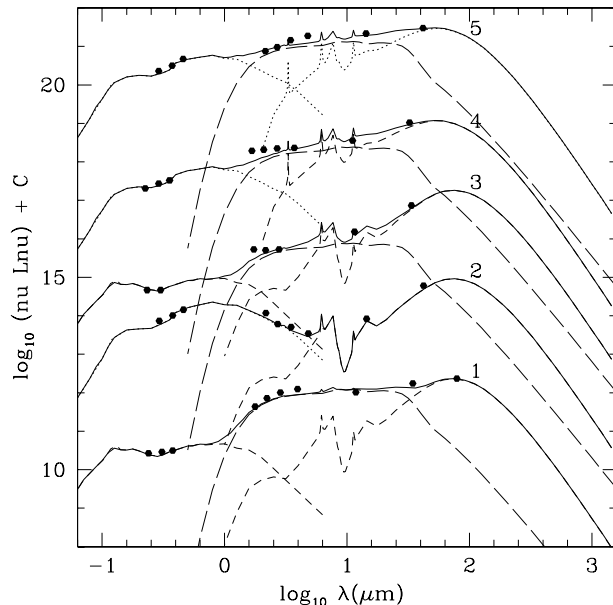


Figure 2. Optical to far-infrared SEDs in νf_ν of all 5 X-ray sources with 70 μ m from CDFS. Solid curves show the total predicted SED. Parameters for model fits given in Table 1.

ber 2005 and March 2006. The data were analysed following the methodology of Laird et al. (2009). The CIAO v3.2 data analysis software was used for the data reduction. After correcting for hot pixels and cosmic ray afterglows using the ACIS_RUN_HOTPIX task, the level 2 event file was produced using ACIS_PROCESS_EVENTS. Flares were identified and removed using the automated method described by Laird et al. (2009). Individual event files although largely overlapping are treated separately to avoid problems arising from merging regions with significantly different PSFs. Images are constructed in four energy bands 0.5–7.0, 0.5–2.0, 2.0–7.0 and 4.0–7.0 keV. Energy weighted exposure maps for each of the four energy bands were constructed using the MERGE_ALL task by adopting a power-law spectrum with spectral index $\Gamma = 1.4$ to estimate the energy weights. For each of the 30 Chandra pointings of the survey, source catalogues were constructed in the energy bands above adopting a Poisson probability threshold of $< 4 \times 10^{-6}$, which are then merged into a master source list following the methodology of Laird et al. (2009). In the case of duplicate sources in the overlap regions of adjacent pointings we keep the detection with the smallest off-axis angle. The count rates in the 0.5–7.0, 0.5–2.0, 2.0–7.0 and 4.0–7.0 keV bands are converted to fluxes in the standard 0.5–10, 0.5–2, 2–10 and 5–10 keV bands respectively assuming a power-law X-ray spectrum with index $\Gamma = 1.4$ and Galactic absorption $N_H = 2 \times 10^{20}$ cm⁻² appropriate for the ELAIS-N1 field. The limiting fluxes are estimated 1.0×10^{-14} , 3.4×10^{-15} and 1.5×10^{-14} erg s⁻¹ cm⁻² in the 0.5–10, 0.5–2 and 2–10 keV bands respectively. A total of 545 unique sources are detected over 1.5 deg² in at least one of the four energy bands to the flux limits above. The second Chandra survey of the ELAIS-N1 is that presented by Manners et al. (2003; 2004). This consists of a single 75 ks Chandra ACIS-I pointing, which lies in middle of our circular geometry shallow survey. Here we use the X-

ray source catalogue produced by these authors. They detect 127 unique sources to flux levels of 2.3×10^{-15} , 9.4×10^{-16} and $5.2 \times 10^{-15} \text{ erg}^{-1} \text{ s}^{-1} \text{ cm}^{-2}$ in the 0.5-8, 0.5-2 and 2-8 keV bands respectively.

2.2 Chandra Deep Field South

The SWIRE CDFS was observed with the MOSAIC II camera on the 4m telescope at Cerro Tololo. Fifteen pointings covered $\sim 4.5 \text{ deg}^2$ in four filters, U, g, r, i to 5σ depths of 24.5, 25.4, 25, 24 magnitudes (Vega) respectively with an additional 1.5 deg^2 survey in the Z filter down to 23.3 magnitudes. There is also a deeper 0.33 deg^2 pointing in U, g, r, i to 5σ depths of 25.2, 25.7, 25.5, 24.5 magnitudes respectively (Lonsdale et al., 2003).

The X-ray data are from the Extended CDFS (ECDFS) and the 1 Ms CDFS. We use the source catalogues of Lehmer et al. (2005) for the ECDFS and Giacconi et al. (2002) for the CDFS. The Extended Chandra Deep Field South consists of 4 ACIS-I pointings covering 0.3 deg^2 with an exposure time of 250 ks each. A total of 592 sources are detected by Lehmer et al. (2005) which reaches sensitivity limits of 1.1×10^{-16} , $6.7 \times 10^{-16} \text{ erg s}^{-1} \text{ cm}^{-2}$ in the 0.5-2 and 2-8 keV bands respectively. The ECDFS is flanking the 1 Ms CDFS survey. Giacconi et al. (2002) have detected 316 X-ray sources down to flux limits of 5.5×10^{-17} , $4.5 \times 10^{-16} \text{ erg s}^{-1} \text{ cm}^{-2}$ in the 0.5-2 and 2-10 keV bands respectively.

2.3 Lockman Hole

The Lockman Hole field was observed in the U, g', r', and i' bands with the MOSAIC Camera at the Kitt Peak National Observatory (KPNO) Mayall 4m Telescope, February 2002 (g', r', and i') and January 2004 (U band). The scale of the Camera is $0.26''/\text{pix}$ and the field of view is $36' \times 36'$. The astrometric mapping of the optical MOSAIC data is good to less than $0.4''$ and the seeing varied between 0.9 and 1.4 arcsec. Data reduction was performed with the Cambridge Astronomical Survey Unit (CASU, Irwin & Lewis 2001) pipeline, following the procedures described in Babbedge et al (2004). Fluxes were measured within a $3''$ aperture (diameter) and corrected to total fluxes using growth curves. Typical 5 sigma magnitude limits are 24.1, 25.1, 24.4 and 23.7 in U, g', r' and i' respectively (Vega), for point-like sources (Berta et al 2007a).

The X-ray data are from the medium deep Chandra survey of Polletta et al (2006). It consists of 9 ACIS-I contiguous pointings of 70 ks each which cover an area of 0.6 deg^2 . The catalogue of Polletta et al (2006) has a total of 827 unique sources to the 0.3-8 keV flux limit of about $10^{-15} \text{ erg s cm}^{-2}$. The total number of Chandra X-ray sources in the three fields is 2091.

3 THE X-RAY/70 μM SAMPLE

In order to identify X-ray sources with $70 \mu\text{m}$ counterparts we have cross-correlated the SWIRE catalogue with the X-ray source lists described above following the same procedure discussed in Fadda et al. (2002), Franceschini et al. (2005) and Polletta et al. (2006). The total number of X-ray/SWIRE sources with $24 \mu\text{m}$ detections is 1368. In order

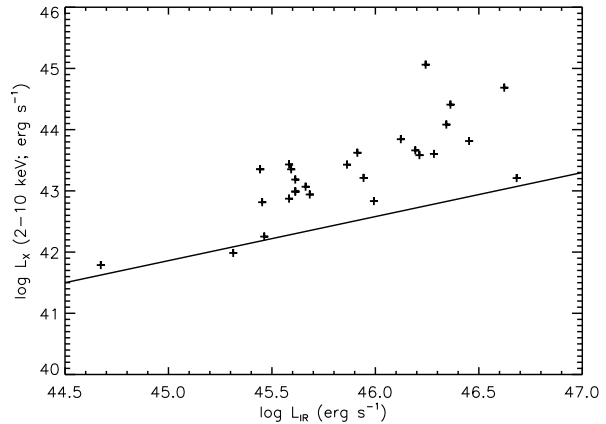


Figure 5. 2-10 keV X-ray luminosity as a function of total IR luminosity, L_{IR} . Black crosses are the X-ray/ $70 \mu\text{m}$ sources. The continuous line is the X-ray/IR luminosity relation for local star-forming galaxies from Ranalli et al. (2003). All X-ray/ $70 \mu\text{m}$ sources deviate from this Ranalli et al. relation in the sense that they are X-ray luminous for their L_{IR} , indicating that AGN activity dominates the X-ray luminosity.

to explore the possible link between AGN activity and star-formation at the epoch close to the peak of AGN luminosity density (e.g. Barger et al. 2005), we further restrict the sample to the redshift interval $0.5 < z < 1.3$ using either spectroscopic (if available) or photometric redshift estimates. This resulted in a total of 28 X-ray/SWIRE sources with $70 \mu\text{m}$ detections. Given the surface density of X-ray and $70 \mu\text{m}$ sources within this redshift interval, the expected number of random associations is < 2 . This sample consists of 5 CDFS sources, 1 from the 1 Ms survey and 4 from the ECDFS, 8 are ELAIS-N1 sources, 7 from the 5ks survey and one from the EDXS and 15 sources are in Lockman. Table 1 gives the positions, redshifts (bracketed if a photometric redshift) and rest-frame luminosities for the different optical, infrared and X-ray components fitted to these sources.

3.1 Multiwavelength Properties

In order to classify the SEDs and estimate photometric redshifts of the sources in our sample, the U-band to $4.5 \mu\text{m}$ photometric data are first fitted using a library of 14 templates, 3 QSO, 1 Starburst and 10 galaxy templates (Rowan-Robinson et al. 2008). Photometric redshifts are estimated at this step. At the longer Spitzer wavebands, the stellar contribution is first subtracted from the photometric data by extrapolating the best fitting galaxy template from the previous step. The corrected 3.6-170 μm data are then fitted with a mixture of four templates, cirrus (quiescent), M82 or Arp220 starbursts, and AGN dust torus, providing information on the nature of sources and the dominant mechanism responsible for the infrared emission, AGN vs stellar processes. The availability of $70 \mu\text{m}$ detections for all 28 sources and $160 \mu\text{m}$ detections for 7 of them is an advantage, providing additional leverage for elucidating the infrared properties of the sample.

For the sample of 28 X-ray/ $70 \mu\text{m}$ sources the minimum number of optical/near-IR bands (up to $4.5 \mu\text{m}$) used for

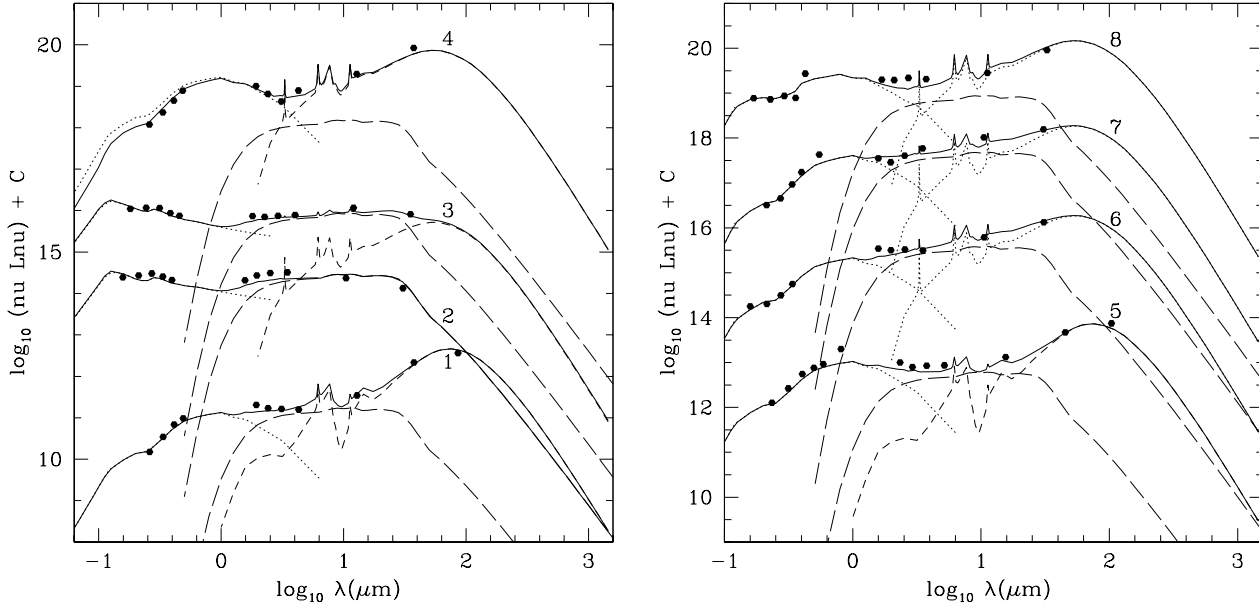


Figure 3. Optical to far-infrared SEDs in νf_ν of all 8 X-ray sources with 70 μ m from ELAIS-N1. Solid curves show the total predicted SED. Parameters for model fits given in Table 1.

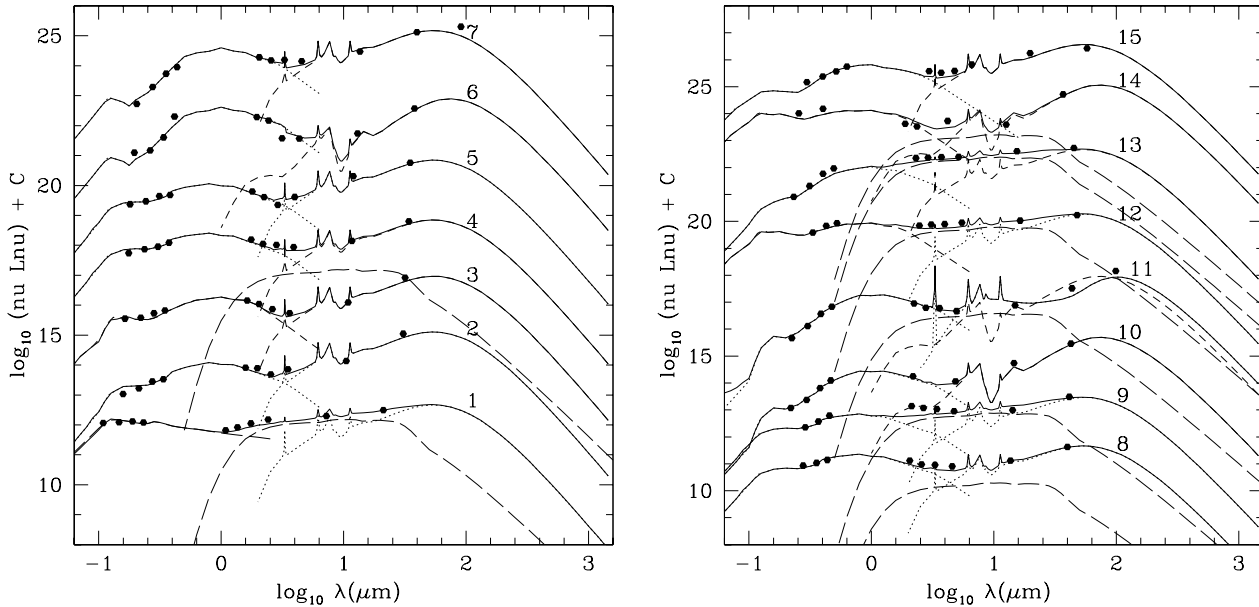


Figure 4. Optical to far-infrared SEDs in νf_ν of all 15 X-ray sources with 70 μ m from Lockman. Solid curves show the total predicted SED. Parameters for model fits given in Table 1.

the photometric redshift calculation is 5. This is sufficient to estimate reliable photometric redshifts. This is demonstrated in Figure 1, which plots photometric against spectroscopic redshift for a total of 12 sources in the sample with optical spectroscopy available either from our own follow-up programs (Trichas et al. in prep.) or from the literature. The agreement is good, with an estimated accuracy of $\delta z / (1 + z_{spec}) \approx 0.02$ for the photometric redshift determinations of the X-ray/70 μ m sources. Broad-band SEDs for all

28 sources are given in Figures 2, 3, 4. The optical galaxy or AGN fits to the U -band to 4.5 μ m data show that the photometric redshift solutions are plausible. All but two of the 28 sources require an M82 or A220 starburst component. The two exceptions are N1-2, which appears to have only an AGN dust torus component in the infrared, and Lockman-11, which seems to be better fitted with a quiescent ('cirrus') component. 19 of the 28 sources require an AGN dust torus component. Since we believe the X-ray emission of all but

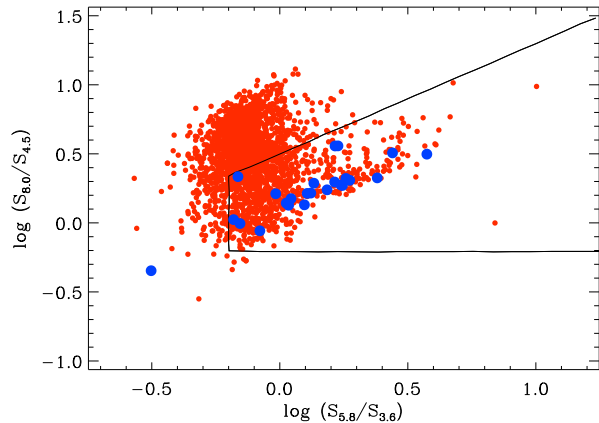


Figure 6. IRAC/MIPS colour-colour plot. Solid line represents the predicted obscured AGN parameter space (Lacy et al., 2004). Red dots are SWIRE 70 μm sources within the redshift interval 0.5-1.3. Blue dots are the 28 X-ray/70 μm sources.

two of the 28 galaxies is due to an AGN (see section 4), the remaining 7 galaxies must be cases with weak dust tori (see discussion by Rowan-Robinson et al. (2009) of the Lockman SWIRE-CLASX sample).

4 RESULTS

The X-ray and mid-IR properties of the X-ray/70 μm sources indicate that most of them host an AGN. Figure 5 shows that the X-ray/70 μm sources are offset to higher X-ray luminosities compared to the Ranalli et al. (2003) $L_X - L_{IR}$ correlation for starbursts. Only two sources in the sample, Lockman-7 and CDFS-2, may possibly be X-ray starbursts, since they have L_X/L_{IR} ratios only slightly higher than the Ranalli et al (2003) mean, and show no evidence for AGN activity (infrared dust torus, broad emission lines, QSO optical SED). Also, the obscuration corrected X-ray luminosities of 26 out of 28 sources in the sample are $L_X(2 - 10 \text{ keV}) \gtrsim 10^{42} \text{ erg s}^{-1} \text{ cm}^{-2}$, higher than what is typically attributed to star-formation (Georgakakis et al. 2007). The X-ray spectra of 19 X-ray/70 μm sources are hard, consistent with column densities $N_H \gtrsim 10^{22} \text{ cm}^{-2}$ (assuming a power-law intrinsic X-ray spectrum with $\Gamma = 1.9$), thereby indicating an obscured AGN. At infrared wavelengths the X-ray/70 μm sources have luminosities $L_{IR} > 10^{11} L_\odot$ and therefore belong to the class of Luminous and Ultra-Luminous Infrared Galaxies (LIRGs, ULIRGs). The template fitting method of section 3 provides information on the emission mechanism(s) that are responsible for these bright luminosities. The mid-IR part of their SEDs include a significant contribution (up to 90 per cent at 8 μm) from a hot dust component associated with AGN activity. This is further demonstrated in Figure 6 which shows the position of the X-ray/70 μm sources on the mid-IR colour-colour plot of Lacy et al. (2004). The majority are in the region of the parameter space occupied by QSOs (Georgantopoulos et al. 2007) and power-law selected AGN (Donley et al. 2008). However, in addition to the contribution from AGN heated dust, our SED modelling also suggests a star-formation component in the mid-IR in almost all cases. This component be-

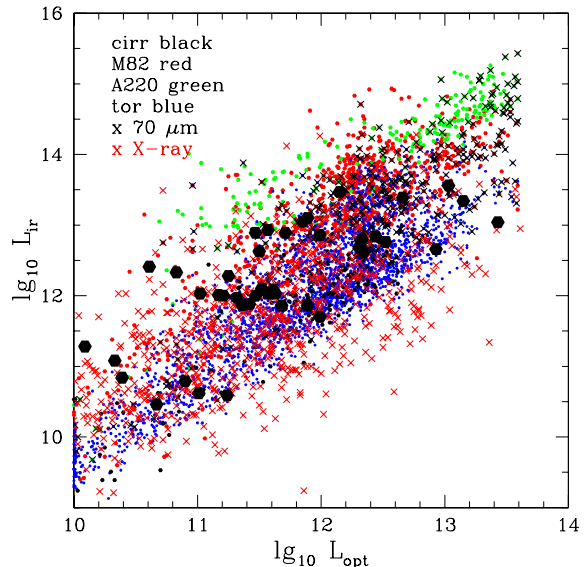


Figure 7. Bolometric infrared luminosity, L_{IR} , versus 0.1-3.0 μm optical luminosity. The small filled circles are SWIRE 24 μm QSOs (black cirrus, red M82, green A220, blue AGN dust torus, data from Rowan-Robinson et al 2008). The black crosses are the subset of these with 70 μm detections. The red crosses are X-ray/SWIRE sources with 24 μm detections (1368 objects). X-ray luminosities are calculated as in RR, Valyanchanov and Nandra 2009. The large black filled hexagons are the subset of these with 70 μm detections.

comes increasingly important at longer infrared wavelengths and is essential to fit the the 70 and/or 160 μm emission of 27 out of 28 sources in the sample. Quantitatively, according to our template fits, for 26 out of 28 sources in Table 1, > 50 per cent of the L_{IR} is from cool dust associated with star-formation. The estimated SFRs are $\gtrsim 50 M_\odot/\text{yr}$, thereby indicating intense starburst events. In summary, the multiwavelength properties of the X-ray/70 μm sources indicate they are systems where both the stellar population and the SBH are growing at the same time. It is interesting to explore whether these two processes are related in the sample sources.

For optically selected QSOs for example, Netzer et al. (2007) and Serjeant & Hatziminaoglou (2009) found that the 60 μm luminosity, which estimates the current star-formation rate, scales with the 5100 \AA continuum luminosity, which is a proxy of the total AGN power, suggesting the two processes are linked. Figure 7 shows an equivalent plot, the bolometric infrared luminosity (L_{IR} ; 3 – 1000 μm) to approximate the luminosity of the current star-formation rate versus the optical bolometric luminosity, L_{opt} (0.1 – 3 μm) for all SWIRE QSOs with 24 μm detections (data from Rowan-Robinson et al 2008), as a proxy of the AGN power (see figure caption for details on the estimation of luminosities). X-ray/70 μm sources and SWIRE QSOs show the same broad correlation between L_{IR} and L_{opt} suggesting an association between the formation of stars in these galaxies and the growth of the SBH at their centres. We note however, that the correlation in Figure 7 has substantial scatter, i.e. at a given L_{opt} the L_{IR} spans about 2 dex. We have also shown the corresponding distribution for the whole sample of SWIRE/X-ray

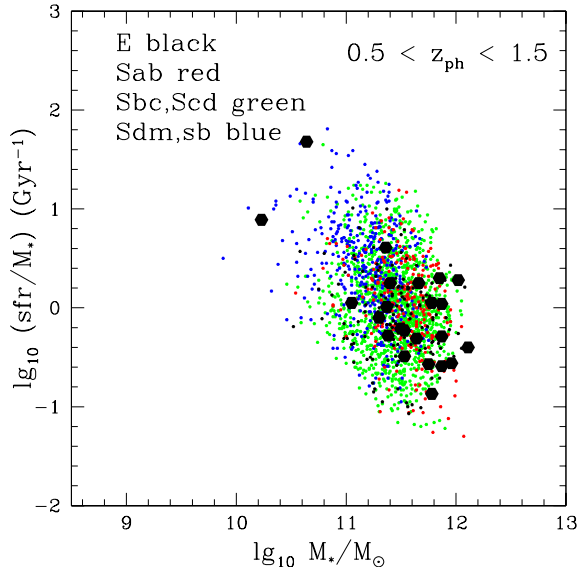


Figure 8. Specific star formation rate in Gyr^{-1} versus stellar mass in $M_{\odot} yr^{-1}$ for SWIRE galaxies, colour-coded by optical template type. The $70\mu m$ /X-ray sources are overplotted as large black filled hexagams. Apart from two objects (CDFS-1 and CDFS-3) at the top left, there is a tendency for our sample to have somewhat high stellar masses ($> 2 \times 10^{11} M_{\odot}$) and somewhat lower specific star formation rates ($< 3 Gyr^{-1}$). Both the two low stellar mass objects in our sample have dust tori.

sources with $24 \mu m$ associations (red crosses in Fig 7), with X-ray luminosities first converted to a bolometric luminosity assuming a bolometric correction to the hard X-ray luminosity of 27, and then to L_{opt} by dividing the bolometric luminosity by 2 (Rowan-Robinson et al 2008). X-ray galaxies with very high values of L_{sb}/L_{opt} are likely to be X-ray starbursts.

In contrast with the $70 \mu m$ QSOs, optically selected samples like the PG QSO samples of Netzer et al (2007) and Lutz et al (2008) are biased towards lower values of L_{sb}/L_{opt} . Optical selection favours objects with higher L_{opt} , $70 \mu m$ selection favours higher L_{ir} . The $70\mu m$ /X-ray sample (filled hexagams in Fig 7) seem to cover the whole range of L_{opt} and L_{ir} .

Figure 8 shows the specific star-formation rate versus stellar mass for the entire SWIRE $70 \mu m$ population, in the redshift interval 0.5-1.5, colour-coded by optical template type, overplotted by our sample. Apart from two objects, CDFS-1 and CDFS-3 with low stellar masses and high specific star-formation rates, the $70\mu m$ /X-ray population is at the lower end of the specific star-formation rate distribution for $0.5 < z < 1.5$, and tends to have a higher stellar masses than the general population, i.e. they avoid the most intense starbursts of similar stellar mass.

It is also interesting that a large fraction of the X-ray/ $70 \mu m$ sample (19/28) are obscured by column densities $N_H \gtrsim 10^{22} cm^{-2}$. Figure 9 compares the HR distribution of the X-ray/ $70 \mu m$ sources with that of the overall X-ray population with SWIRE photometric redshifts in the interval 0.5–1.5. A Kolmogorov-Smirnov tests shows that the likelihood of the observed differences if the two samples are drawn from the same parent population is about 3 per cent. Therefore there

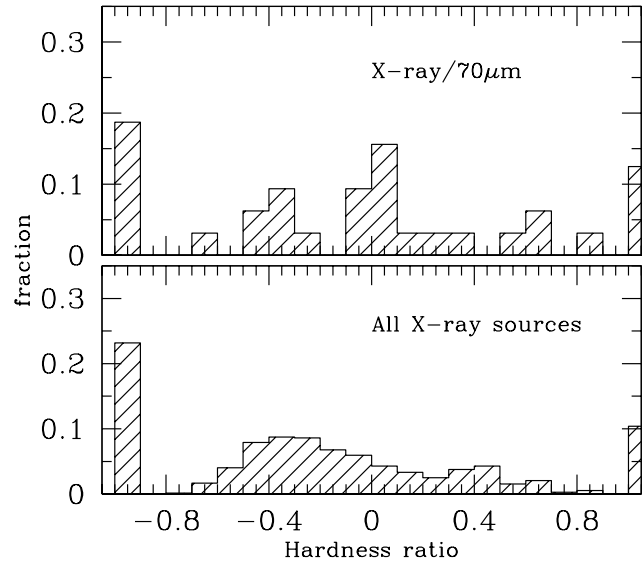


Figure 9. Hardness ratio distribution for X-ray/ $70 \mu m$ sources and the entire X-ray source population identified with SWIRE sources in the redshift interval. The hardness ratio is defined as $HR=(H-S)/(H+S)$ where H is the hard band (2-7keV) count rate and S is the soft band (0.5-2 keV) count rate. The KS test shows that the probability that the distribution are drawn from the same parent samples is 3%, i.e. there are no statistically significant ($< 2\sigma$) differences between the two populations.

is no strong evidence (3 per cent or about 2σ in the case of a normal distribution) that the X-ray/ $70 \mu m$ sources are more obscured than the overall X-ray population.

5 DISCUSSION

Chandra X-ray data within the SWIRE survey footprint are used to select a total of 28 X-ray sources with detections at $70 \mu m$, with additional $160\mu m$ for 25% of them, in the redshift interval 0.5-1.3 to study the properties of galaxies that are best candidates for systems where the formation of the stellar population is taking place at the same time as the growth of the SBH at their centres. Study of the multiwavelength U-band to far-IR SED of these systems indeed shows that the majority of the sample harbors powerful starbursts (27/28; $\gtrsim 50 M_{odot}/yr$), while the X-ray data indicate AGN activity in at least 26/28 sources.

The X-ray spectra of 19/28 sources are consistent with moderate obscuration, $N_H \gtrsim 10^{22} cm^{-2}$. However, the obscured AGN fraction in the sample is similar to that of the overall X-ray AGN population in the same redshift interval. This contradicts some models for the co-evolution of AGN and galaxies in which the central engine is obscured by dust and gas clouds associated with circumnuclear starbursts (e.g. Fabian et al. 1999; Hopkins et al. 2006; Ballantyne 2008). Alternatively, our finding may indicate that a substantial fraction of the AGN has ongoing star-formation and that the X-ray/ $70 \mu m$ might not be very different in their star-formation

properties from the bulk of the X-ray AGN population. Silverman et al. (2009) for example, used the [OII] 3727 line as proxy of the star-formation rate in X-ray selected AGN at $z \approx 1$ and showed that the majority show evidence for star-formation.

We also find that X-ray/ $70 \mu\text{m}$ avoid the most intense starbursts at a given stellar mass. This is consistent with models where outflows from the central engine moderate the star-formation by sweeping away the cold gas reservoirs of the host galaxy (e.g. Hopkins et al. 2006). This result also contradicts Silverman et al. (2009) who finds that X-ray selected AGN in the COSMOS field have, on average, higher star-formation rate compared to non X-ray sources in that field of similar stellar mass.

6 CONCLUSION

SWIRE infrared and optical data have been combined with Chandra X-ray observations in the ELAIS-N1, Lockman Hole and CDF-S to study the nature of the X-ray/ $70 \mu\text{m}$ sources in the redshift interval 0.5-1.3. The majority of these systems are starburst/AGN composites thereby providing the opportunity to explore the relation between SBH growth and galaxy formation. The X-ray/ $70 \mu\text{m}$ sources follow the broad correlation between star-formation rate (approximated by the L_{IR}) and SBH accretion rate (approximated by L_{opt}) for broad line QSOs, suggesting that these two processes are linked. We do not find evidence that the X-ray/ $70 \mu\text{m}$ are more obscured than the overall X-ray population, contrary to the predictions of some AGN/starburst co-evolution models. Also, the X-ray/ $70 \mu\text{m}$ population appears to avoid the most intense starbursts for their stellar mass. This may indicate AGN driven moderation of the star-formation in the host galaxy.

7 ACKNOWLEDGMENTS

The authors wish to thank Elise Laird and James Aird for their assistance in reducing Chandra data and the SWIRE team for their constructive comments on the original Chandra ELAIS-N1 proposal. This work has been supported by funding from the Peren grant (MT) and the STFC Rolling grant (MT).

REFERENCES

- Alexander, D. M., et al., 2005, *Nature*, 434, 738
 Babbedge, T. S., R., et al, 2004, *MNRAS*, 353, 654
 Ballantyne, D., 2008, *ApJ*, 685, 787
 Barger, A. J., et al., 2005, *AJ*, 129, 578
 Berta, S., et al., 2007, *A&A*, 467, 565
 Blanton M., 2006, *ApJ*, 645, 268
 Cid Fernandes, R., et al., 2001, *ApJ*, 558, 81
 Donley, J., et al., *ApJ*, 687,111
 Fabian, D., et al., *MNRAS*, 308, 39
 Fadda, D., et al., 2002, *A&A*, 383, 838
 Fazio, G., et al., 2004, *ApJS*, 154, 10
 Ferrarese, L. et al., 2000, *ApJ*, 539, 9
 Franceschini, A., et al., 2005, *AJ*, 129, 2074
 Gebhardt, K. et al., 2000, *ApJ*, 543, 5
 Georgakakis, A., et al., 2007, *MNRAS*, 377, 203
 Georgakakis, A., et al., 2008, *MNRAS*, 388, 1205
 Georgantopoulos, I., et al., 2007, *A&A*, 466, 823
 Giacconi, R., et al., 2002, *ApJS*, 139, 369
 Grogin, N. A., et al., 2003, *ApJ*, 595, 685
 Hasinger, G., et al., 2005, *A&A*, 441, 417
 Hopkins, P. et al., 2005, *ApJ*, 630, 705
 Hopkins, P. et al., 2006, *ApJ*, 652, 864
 Hopkins, P. et al., 2007, *ApJ*, 659, 976
 Irwin, M., et al., 2001, *NewAR*, 45, 105
 Kauffmann, G., et al., 2003, *MNRAS*, 353, 713
 Lacy, M., et al., 2004, *ApJS*, 154, 166
 Laird, E., et al., 2009, *ApJS*, 180, 102
 Lehmer, B., et al., 2005, *ApJS*, 161, 21
 Lonsdale, C., et al., 2003, *PASP*, 115, 897
 Lutz, D., et al., 2008, *ApJ*, 684, 853
 Magorrian, J. et al., 1998, *AJ*, 115, 2285
 Manners, J., et al., 2003, *MNRAS*, 343, 293
 Manners, J., et al., 2004, *MNRAS*, 355, 97
 McMahon, R., et al., 2001, *NewAR*, 45, 97
 Nandra, K. et al., 2007, *ApJ*, 660, 11
 Netzer, H., et al., 2007, *ApJ*, 671, 1256
 Page, M. J., et al., 2004, *ApJ*, 611L, 85
 Pierce, C. M., et al., 2007, *ApJ*, 660L, 19
 Polletta, M., et al., 2006, *ApJ*, 642, 673
 Ranalli, P., et al., 2003, *A&A*, 399, 39
 Rieke, G., et al., 2004, *ApJS*, 154, 25
 Rowan-Robinson, M., et al., 2005, *AJ*, 129, 1183
 Rowan-Robinson, M., et al., 2008, *MNRAS*, 386, 697
 Rowan-Robinson, M., et al, 2009, *MNRAS*, submitted
 Silverman, J., et al., 2009, *ApJ*, 696, 396
 Serjeant, S. & Hatziminaoglou, E., 2009, *MNRAS*, tmp, 782S
 Surace, J., et al., 2005, *AAS*, 207, 6301